Genetic and phylogenetic analysis of dissimilatory iodate-reducing bacteria identifies potential niches across the world's oceans

Victor Reyes-Umana[1], Zachary Henning[1], Kristina Lee[1], Tyler P. Barnum[1], John D. Coates[1]
[1]Department of Plant and Microbial Biology, University of California, Berkeley, CA 94720, USA

Abstract

Iodine is oxidized and reduced as part of a biogeochemical cycle that is especially pronounced in the oceans, where the element naturally concentrates. The use of oxidized iodine in the form of iodate (IO_3^-) as an electron acceptor by microorganisms is poorly understood. Here, we outline genetic, physiological, and ecological models for dissimilatory IO_3^- reduction to iodide (I^-) by a novel estuarine bacterium, *Denitromonas iodocrescerans* strain IR-12, *sp. nov*. Our results show that dissimilatory iodate reduction (DIR) by strain IR-12 is molybdenum-dependent and requires an IO_3^- reductase (*idrA*) and likely other genes in a mobile cluster with a conserved association across known and predicted DIR microorganisms (DIRM). Based on genetic and physiological data, IO_3^- is likely reduced to hypoiodous acid (HIO), which rapidly disproportionates into IO_3^- and iodide (I^-), in a respiratory pathway that provides an energy yield equivalent to that of nitrate or perchlorate respiration. Consistent with the ecological niche expected of such a metabolism, *idrA* is enriched in the metagenome sequence databases of marine sites with a specific biogeochemical signature and diminished oxygen. Taken together, these data suggest that DIRM help explain the disequilibrium of the IO_3^-:I^- concentration ratio above oxygen minimum zones and support a widespread iodine redox cycle mediated by microbiology.

Introduction

Iodine (as ^{127}I) is the heaviest stable element of biological importance and an essential component of the human diet due to its role in thyroxine biosynthesis in vertebrates[1-3]. Iodine is enriched in marine environments where it exists in several oxidation states, reaching concentrations of up to 450 nM[4]. In these environments, organisms such as kelp bioconcentrate iodine as iodide (I^-) and produce volatile iodine species such as methyl iodide[5]. These volatile iodine species contribute to the destruction of tropospheric ozone (a major greenhouse gas) and aerosol formation at the marine boundary layer, consequently resulting in cloud formation and other local climatic effects[1,6]. Despite the global biological and geochemical importance of iodine, little is known about its biogeochemistry in the ocean[4]. For instance, the biological mechanism accounting for the unexpected chemical disequilibrium between I^- and iodate (IO_3^-) in seawater (I^-:IO_3^- disequilibrium) remains unknown[4]. At the physicochemical conditions of seawater, iodine is most stable as IO_3^- [7], yet measurements of IO_3^- and I^- in regions with high biological productivity (e.g., marine photic zones, kelp forests, or sediments), reveal an enrichment of the I^- ion beyond what can be explained through abiotic reduction[7,8].

Among numerous explanations proposed for I^- enrichment, microbial IO_3^- reduction is particularly compelling. The high reduction potential (IO_3^-/I^- E_h = 0.72V at pH 8.1)[7,9] makes IO_3^- an ideal electron acceptor for microbial metabolism in marine environments. Early studies indicated

common microorganisms such as *Escherichia coli* and *Shewanella putrefaciens,* reduce IO_3^- to I^- [9,10]. Subsequent studies associated this metabolism with the inadvertent activity of DMSO respiratory reductase enzymes in marine environments, along with specific enzymes (i.e., perchlorate reductase, nitrate reductase) that reduce IO_3^- *in vitro* [9,11,12]. However, there is little evidence that organisms hosting these enzymes are capable of growth by IO_3^- reduction. While inadvertent IO_3^- reduction might be mediated by marine bacteria possessing DMSO reductases, until recently, no definitive evidence existed that global IO_3^- reduction is a microbially assisted phenomenon.

In support of a microbial role for the observed I^-:IO_3^- disequilibrium, previous studies demonstrated that at least one member each of the common marine genera *Pseudomonas* and *Shewanella* are capable of IO_3^- reduction[12-14]. More recently, IO_3^- reduction by *Pseudomonas* sp. strain SCT was associated with a molybdopterin oxidoreductase closely related to arsenite oxidase[14]. As part of this work, a dedicated biochemical pathway was proposed involving two peroxidases associated with a heterodimeric IO_3^- reductase (Idr)[14]. The putative model proposes a four-electron transfer mediated by Idr, resulting in the production of hydrogen peroxide and hypoiodous acid[14]. Two peroxidases detoxify the hydrogen peroxide while a chlorite dismutase (Cld) homolog dismutates the hypoiodous acid into I^- and molecular oxygen, which is subsequently reduced by the organism[14]. The proposed pathway involving a molecular O_2 intermediate is analogous to canonical microbial perchlorate respiration[15]. By contrast, Toporek *et al.*[18] using the IO_3^- respiring *Shewanella oneidensis* demonstrated the involvement of a multiheme cytochrome not found in *Pseudomonas* sp. strain SCT suggesting an alternative DIR pathway. The disparate mechanisms underscore the potential diversity of IO_3^- respiratory processes. As such, identification of additional DIR microorganisms (DIRM) would clarify which genes are required for this metabolism and enable identification of IO_3^- respiratory genes in metagenomes.

With this as a primary objective, we identified a novel marine DIRM, *Denitromonas iodocrescerans* strain IR-12, *sp. nov,* that obtained energy for growth by coupling IO_3^- reduction to acetate oxidation. Taxonomic analysis placed this organism in the *Denitromonas* genus commonly associated with marine environments[19]. We used comparative genomics to identify the core genes involved in IO_3^- respiration, which formed a distinct mobile genomic island. Reverse genetics, physiology, and comparative genomic data were used to propose a new model for DIR, with a confirmed role for a molybdopterin-dependent IO_3^- reductase (IdrAB)[14]. A phylogenetic analysis was used to establish the distribution of this metabolism across the tree of life and measure the degree to which the genomic island is subject to horizontal gene transfer. Finally, metagenomic analysis identified the *idrA* gene in the Tara oceans datasets, enabling the correlation of DIR populations with ocean chemistry. These results together enabled the proposed model for the global distribution of the DIR metabolism and the ecology of the microorganisms involved.

Results and discussion

Isolation of *D. iodocrescerans*

D. iodocrescerans was isolated under anoxic conditions from estuarine sediment samples by selective enrichment followed by single colony isolation on agar plates. Analysis of the 16S rRNA

indicated an axenic culture composed of a single phylotype (strain IR12) belonging to the *Denitromonas* genus in the beta proteobacteria identical to an uncultured *Denitromonas* clone from a metagenomic sample (GenBank: KF500791.1) (Figure 1A). The closest cultured relatives were *D. indolicum* strain MPKc[20] (GenBank: AY972852.1, 99.46% similarity) and *D. aromaticus* (GenBank: AB049763.1, 99.40% similarity). Morphologically, strain IR12 is a rod-shaped motile cell 1-2 μm long and 0.5 μm diameter with a single polar flagellum (Figure 1B). Based on its phylogenetic affiliation, morphology, and metabolism (described below) we propose that strain IR12 represents a new species in the *Denitromonas* genus with the epitaph *D. iodocrescerans.*

Physiology and energetics of *D. iodocrescerans*

Cells of *D. iodocrescerans* grew on basal medium with acetate and IO_3^- as the sole electron donor and acceptor, respectively (Figure 1C and D). Ion chromatography and growth studies revealed that IO_3^- was quantitatively reduced to I^- with concomitant cell density increase. No growth or acetate consumption occurred in the absence of IO_3^-. Similarly, no IO_3^- reduction occurred in the absence of acetate or in heat killed controls. These results indicated that IO_3^- reduction was enzymatically mediated coupled to acetate oxidation and growth. Acetate-free control cultures reduced micromolar amounts of IO_3^- (114 ± 34 μM, mean ± standard deviation, n=3) which was attributable to residual acetate carried over from the inoculum (**Error! Reference source not found.**). *D. iodocrescerans* consumed 2.46 ± 0.499 mM IO_3^- (mean ± standard deviation, n=3) while oxidizing 2.86 ± 0.427 mM acetate (mean ± standard deviation, n=3) with a final optical density (OD_{600}) increase of 0.109. This is equivalent to an average stoichiometry of 0.86 mol IO_3^- per mol acetate. The morphological consistency between *D. iodocrescerans* and *E. coli*, suggests that an OD_{600} increase of 0.39 is equivalent to 1 gram of cell dry weight[21] and that ~50% of cell dry weight is comprised of carbon[22]. Using these numbers, the corrected stoichiometry accounting for acetate incorporation into cell mass is 93% of the theoretical value according to:

$$3\ CH_3COOH + 4\ IO_3^- \rightarrow 6\ CO_2 + 4\ I^- + 6\ H_2O$$

Our calculations indicate that 30.72% of total carbon is assimilated into biomass while the remaining is respired. Such a result is typical for highly oxidized electron acceptors such as oxygen, nitrate, or perchlorate[15,23]. In support of this, the calculated Gibb's free energy and the change in enthalpy for the reduction of IO_3^- per mole of electrons transferred is -115 kJ/mol e^- and -107 kJ/mol e^- respectively[24]. These values place the energy provided through IO_3^- respiration akin to that of perchlorate respiration (ClO_4^-/Cl^-, $E^{o\prime}$ = +0.797 V) [15], and between that of aerobic respiration (O_2/H_2O, $E^{o\prime}$ = +0.820 V) and nitrate reduction (NO_3^-/N_2, $E^{o\prime}$ = +0.713 V)[25]. This suggests a similar degree of carbon assimilation would be expected for IO_3^- respiration [23].

DIR is molybdate dependent

The reduction of oxyanions like IO_3^-, such as bromate, chlorate, perchlorate, and nitrate, is typically catalyzed by enzymes belonging to the DMSO reductase superfamily of molybdopterin oxidoreductases[26]. These enzymes require molybdenum as a cofactor in order to donate two

electrons at a time to the receiving molecule[27]. To determine if phenotypic IO_3^- reduction was molybdenum-dependent, we passaged *D. iodocrescerans* six times in aerobic, molybdate-free minimal media to remove any trace molybdenum as described in Chaudhuri *et al* [28]. As expected, and similarly to observations with perchlorate reducing microorganisms [28], omitting molybdenum from the oxic medium did not affect the aerobic growth of *D. iodocrescerans* (data not shown). In contrast, no growth or IO_3^- reduction was observed when these cells were passaged into molybdenum-free anoxic media with IO_3^- as the electron acceptor (Figure 1E). When 0.1mM sodium molybdate was added into the non-active cultures at 14 hours post inoculation, growth and IO_3^- resumed (Figure 1E). These results demonstrate that IO_3^- respiration by *D. iodocrescerans* is molybdenum dependent and are consistent with the involvement of a DMSO oxidoreductase in IO_3^- reduction[28].

Core genes required for DIR

To identify the genes required for IO_3^- respiration we performed a comparative genomic analysis between the genomes of the IO_3^- respiring species (*D. iodocrescerans* and *Pseudomonas* sp. SCT), and the non-IO_3^- respiring close relatives (*D. halophilus* SFB-1, and *Pseudomonas* sp. CAL). Additionally, *Pseudomonas* and *Denitromonas* form phylogenetically distinct genera (*Gammaproteobacteria* and *Betaproteobacteria,* respectively), reducing the likelihood of shared gene content[29]. We surmised that DIRM must share a unique gene (or set of genes) that enables IO_3^- reduction. This comparison identified 26 genes uniquely shared by the two DIRM and not found in the closely related non-IO_3^- respiring species (Figure 2A; Table S2). Four of these genes were present in a gene cluster that contained genes for alpha and beta subunits of a DMSO reductase family molybdopterin enzyme related to arsenite oxidase (AioAB)[30] supporting our result of a molybdenum dependency for this metabolism. The remaining two genes in the cluster were closely related to cytochrome C peroxidases *ccp1* and *ccp2*, possibly involved electron shuttling and oxidative stress responses[31,32]. These four genes were similar to those identified by Yamazaki *et al.* under the proposed nomenclature *idr*A, *idr*B, *idr*P_1, *idr*P_2 for *Pseudomonas* sp. SCT[14] (Figure 2B). A SignalP analysis showed that *idr*P_1 and *idr*P_2 possessed a signal sequence for periplasmic secretion via the Sec pathway, while *idr*B used the Tat pathway[33]. By contrast *idr*A did not have a signal peptide sequence, suggesting its protein product is co-transported with IdrB into the periplasm[34]. Based on this evidence, we concluded that dissimilatory IO_3^- reduction in *D. iodocrescerans* occurs entirely in the periplasm, consistent with the observation by Amachi *et al*. that associated IO_3^- reductase activity in the periplasmic fractions of *Pseudomonas* strain SCT [13]. Notably, the gene cluster lacked a quinone oxidoreductase suggesting that *D. iodocrescerans* involves the expression of a non-dedicated quinone oxidoreductase.

Evidence associating IdrAB to DIR, currently relies on the IO_3^- consuming activity of crude cell extracts of *Pseudomonas* strain SCT and differential expression of *idrABP*$_1$*P*$_2$ under IO_3^- reducing conditions[14]. To validate the association between these genes and DIR in *D. iodocrescerans*, we developed a genetic system to perform targeted knockouts (see Table S1 and supplemental methods for details). The *idrA* gene was targeted since its associated molybdenum cofactor ultimately mediates the reduction of the oxyanion[26]. Upon introduction of an in-frame deletion at the *idrA* locus, the organism was incapable of growth via IO_3^- respiration (Figure 2C) while growth under oxic conditions remained unimpaired. Complementation of *idrA* on a low copy number

vector (pVR065) restored the IO_3^- respiring phenotype demonstrating that the *idrA* gene is a prerequisite to enable IO_3^- respiration (Figure 2C). Our identification of a second DIRM, in addition to *Pseudomonas* strain SCT, with an IdrAB suggests that IO_3^- reduction requires a specialized molybdopterin oxidoreductase, and that other molybdopterin oxidoreductases in the genome cannot rescue the phenotype. Furthermore, our work demonstrates a distinct difference from IO_3^- reduction by the multiheme cytochrome in *Shewanella* and suggests that the ability to reduce IO_3^- may have evolved at least twice independently.

An alternative DIR model

The current model for IO_3^- respiration by *Pseudomonas* strain SCT proposes the donation of electrons from the quinone pool via a cytochrome c to IdrAB, to initiate reduction of IO_3^- to HIO and H_2O_2. H_2O_2 is reduced to H_2O by the peroxidases $IdrP_1$ and $IdrP_2$, while a chlorite dismutase (Cld)-like enzyme converts HIO to I^- and $½O_2$, a catalytic function that has never been demonstrated for Cld or Cld-like proteins[14]. The resultant oxygen is then further respired to H_2O by a terminal oxygen reductase. The putative participation of a Cld-like protein was based on expression data rather than empirically determined activity[14]. Furthermore, comparative genomics does not support the general involvement of Cld in IO_3^- respiration, as *cld* is never co-located with the IRI and is notably absent from all but two of the 145 putative DIRM genomes identified in NCBI GenBank (see below) including the genome of *D. iodocrescerans*.

Since *D. iodocrescerans* genome lacks *cld*-like genes, we propose that the primary mechanism of IO_3^- respiration by this organism relies on the complex and reactive chemistry of iodine oxyanions[35] and that the peroxidases $IdrP_1$ and $IdrP_2$ serve a critical detoxification role for inadvertent oxidants generated rather than being central components of the pathway itself. In the *D. iodocrescerans* model (**Figure 3**A), IdrAB accepts electrons from cytochrome c551, and performs a four-electron transfer, similarly to the mechanism of perchlorate reductase (Pcr)[36], with a resultant production of the chemically unstable intermediate hypoiodous acid (HIO). This intermediate then undergoes abiotic disproportionation to yield I^- and IO_3^- as reported in alkaline aquatic environments[16,37], and is simplistically represented by the following equation:

$$3\ HIO \rightarrow 2\ I^- + IO_3^- + 3\ H^+$$

The resultant IO_3^- subsequently cycles back into the reductive pathway. In this manner, the cell completes the 6-electron reduction of IO_3^- to I^- without invoking a Cld-like enzyme with putative capacity to dismutate IO^- to I^- and O_2. This model is similar to the cryptic model for some species of perchlorate reducing microorganism which rely on the chemical reactivity of the unstable pathway intermediate chlorite (ClO_2^-) with reduced species of iron or sulfur to prevent toxic inhibition [36,38]. We propose that the initial reduction of IO_3^- at the IdrA inadvertently produces low levels of incidental toxic H_2O_2. This is analogous to the production of hypochlorite (ClO^-) by respiratory perchlorate reducing microorganisms during respiration of perchlorate or chlorate[39,40]. To protect themselves from this reactive chlorine species, perchlorate respiring organisms have evolved a detoxifying mechanism based on redox cycling of a sacrificial methionine rich peptide[40]. In the *D. iodocrescerans* model for IO_3^- respiration the cytochrome c peroxidases play the critical detoxification role against inadvertent H_2O_2 production, rather than a central role for the reductive

pathway as proposed for *Pseudomonas* strain SCT[14] (**Figure 3**A). Such a model is not only parsimonious with the predicted biochemistries and abiotic reactivities of the proteins and iodine oxyanions involved but is also consistent with the micromolar quantities of H_2O_2 observed by Yamazaki *et al.* during the reduction of millimolar quantities of IO_3^- by *Pseudomonas* strain SCT[14].

Evolutionary history of DIR

Core genes for DIR were used to define the phylogenetic distribution of this metabolism. Close homologs to the catalytic subunit of IdrA were identified among genomes in NCBI GenBank. A phylogenetic tree of the DMSO reductase family (Figure 4A and 4B) confirms previous results indicating that arsenite oxidase alpha subunit (AioA) is the most closely related characterized enzyme to IdrA[14]. The extent of the IdrA clade was difficult to define because IdrA from *D. iodocrescerans* and *Pseudomonas* sp. SCT are closely related. To determine whether more IdrA homologs in this clade function as IO_3^- reductases or arsenite oxidases, we performed a gene neighborhood analysis looking at the 10 genes both upstream and downstream of either the *idrA* or *aioA* locus and clustered them using MMseqs2[41] (Figure 5). We observed a clear distinction in neighborhood synteny between genes mostly closely to *idrA* versus those most closely related to *aioA*. All neighborhoods in the *idrA* clade showed conserved synteny at *idrABP$_1$P$_2$* (Figure 5), whereas organisms with an AioA, showed an alternative gene structure, notably missing the cytochrome c peroxidases. Based on this pattern, all organisms possessing *idrABP$_1$P$_2$* genes are likely DIRM. The outgroups of IO_3^- reductase in this phylogeny are homologs found in *Halorubrum* spp., which are known to oxidize arsenite[42], and a *Dehalococcodia* bacterium (GCA_002730485.1), which also lacks the cytochrome c peroxidases in its gene neighborhood (Figure 5). Further research into these proteins may provide more information on the transition from arsenite oxidase to IO_3^- reductase.

Genes mediating IO_3^- reduction were identified in 145 genomes from bacteria in the *Alphaproteobacteria*, *Betaproteobacteria*, and *Gammaproteobacteria*. Deeper branching members included members of *Planctomycetaceae* and several others belonging to the Candidate Phyla Radiation group such as, *Ca. Rokubacteria*, *Ca. Lindowbacteria*, and NC10 (Figure 4B)[43-45]. DIR seemed most prevalent in the phylum *Proteobacteria*, which is a pattern that has been observed for some other rare metabolisms[46]. The discordance between the taxonomy of the host organisms and the phylogeny of IdrA (Figure 4B; Figure S1)[47] suggested that DIR is a horizontally transferred metabolism. For example, IdrA in the *Gammaproteobacterium Pseudomonas* sp. SCT was most closely related to IdrA in *Betaproteobacteria* such as *Azoarcus sp.* DN11. Additional evidence for horizontal gene transfer in individual genomes included insertion sites at the 3' end of tRNAs, a skew in GC content, and association with other horizontally transferred genes[48,49]. In *D. iodocrescerans*, there was no significant GC skew, but we observed a $tRNA^{Gly}$ roughly 72 kbp downstream of the *idrABP$_1$P$_2$* locus. While we did not detect inverted repeats, Larbig *et al.* previously demonstrated an integration site in *P. stutzeri* at $tRNA^{Gly50}$. Additionally, numerous heavy metal resistance markers, like *mer* and *cus* genes, were found near the *idrABP$_1$P$_2$* locus (1.2 kbp and 22 kbp away respectively), further suggesting horizontal transfer[48,51,52]. A method to detect genomic islands in complete genomes predicted the *idrABP$_1$P$_2$* locus to be its own 5.8 kbp genomic island in *Azoarcus* sp. DN11, which has a complete genome and a closely related IdrA. Therefore, while there is poor conservation of genes surrounding *idrABP$_1$P$_2$* and questions remain about its

recent evolution, the high degree of conservation of *idrABP$_1$P$_2$* locus itself and the phylogenetic pattern of inheritance support its description as an iodate reduction genomic island (IRI) that is subject to horizontal gene transfer. In addition to the perchlorate reduction genomic island (PRI)[46] the IRI represents one of the few respiratory genomic islands known that crosses large phylogenetic boundaries (class, order, and family).

Distribution of DIR populations in global oceans

Many of the organisms with genes for DIR were identified in diverse marine habitats where IO_3^- reduction is suspected to occur (Table 3). For example, *Litorimicrobium taeanense* is an aerobic, non-motile, *Alphaproteobacterium* isolated from a sandy beach in Taean, South Korea[53]. Other organisms such as *Endozoicomonas sp.* OPT23 and *Litoreibacter ascidiaceicola* were isolated from marine animals such as the intertidal marine sponge (*Ophlitaspongia papilla*) and the sea squirt (*Halocynthia aurantium*), respectively[54,55]. Additionally, organisms known to accumulate iodine, such as algae[56] are associated with these bacteria as is the case with the bacterium *Rhodophyticola porphyridii* and the red algae *Porphyridium marinum*[57]. To investigate this marine prevalence further we used the *idrA* subunit as a marker gene to determine DIRM distribution across the Tara Oceans metagenome dataset. Our approach also identified the read abundance mapping to these unique IdrA hits at the different sites by using the transcripts per million (TPM) method for read quantification[58,59]. With this method, the number of unique IdrA hits was directly proportional to the number of reads mapped to the hits (Figure 6A and 6B). In general, locations with few unique IdrA hits lacked reads mapping to IdrA (Figure 6B). We observed that 77% (74/96) of the hits arose from the mesopelagic zone at an average depth of about 461 meters (range 270m-800m) across identified stations (Figure S2). The remaining hits arose predominantly in epipelagic zones, such as the deep chlorophyll maximum in 21% of cases (20/96) and far fewer hits were observed in the mixed layer (1/96) or the surface water layer (1/96).

Although the presence of *idrA* exhibited some variability in depth, a geochemical feature common to all these hits was low oxygen concentrations. The vast majority of hits mapped to well-documented oxygen minimal zones in the Arabian Sea[60,61] and the Eastern Tropical Pacific[62-64]. Similarly, the North Pacific Subtropical and Polar Front (MRGID:21484) and the North Pacific Equatorial Countercurrent provinces (MRGID:21488) are two Longhurst provinces with OMZs that stand out in the Western hemisphere. At each of these locations, the median dissolved oxygen concentration at *idrA* positive locations was consistently lower than the dissolved oxygen concentrations at *idrA* absent locations (65.24 µmol/kg versus 190.41 µmol/kg; Figure 6E). Among locations containing more than one *idrA* hit, the average oxygen concentration was about six times lower (11.03 µmol/kg); however, this average was skewed upward due to one outlier condition with 18 *idrA* hits (Cumulative TPM of 89.30; Figure S2) occurring at a dissolved oxygen concentration of 95.4 µmol/kg (TARA_137_DCM_0.22-3). Environments meeting these conditions were the most common in mesopelagic zones broadly. One notable exception were the multiple hits at the deep chlorophyll maximum (DCM) at station 137. However, further inspection of the physical environment at the DCM revealed that this station matched mesopelagic environments more closely than surface waters or deep chlorophyll maxima. Research from Farrenkopf *et al.* indicated that bacteria are responsible for IO_3^- reduction in oxygen minimum zones[12,65]. Further, Saunders *et al.* showed a preferential expression of AioA-like genes in the

Eastern Pacific oxygen minimum zones, which our evidence now suggests are IO_3^--reductases (IdrA)[30].

To test whether locations with *idrA* possessed a unique chemical signature, we ran a principal component analysis using the variables associated with sample environments. Together the first two components of these geochemical variables explained 70.66% of the variance observed between *idrA* present and *idrA* absent samples. We determined that *idrA* presence was correlated most strongly with increased nitrate, phosphate, and silicate concentrations (Figure 6C-E). Additionally, *idrA* presence was negatively correlated with dissolved oxygen concentrations (Figure 6C-E). Such an observation is atypical for highly productive nitrate and phosphate depleted OMZs[60,66,67]. A possible explanation for this observation is that DIRM inhabit a unique niche above OMZs where residual O_2 prevents *fnr*-dependent expression of nitrate reductase[68]. Organisms in these environments could potentially use IO_3^- as an alternative electron acceptor. Excess phosphorous in these zones seemingly serves as a proxy indicator of lower overall productivity, and potentially reflects the limiting concentration of IO_3^- and oxygen for biomass accumilation[4,23]. Our explanation corroborates results from Farrenkopf *et al.* that shows an I^- maximum occurring at the boundary of the OMZ[61], but further studies into the biochemistry of IO_3^- reduction under suboxic conditions and the contribution of DIRM to I^- formation at this transition zone are necessary to undeniably link the I^- maximum with the presence of *idrA* directly.

Significance

Here we describe a new organism, *Denitromonas iodocrescerans*, that grows by IO_3^- respiration which is mediated by a novel molybdenum dependent DMSO reductase. The conserved core genes associated with DIR and the chemistry of iodine oxyanions are consistent with a hybrid enzymatic-abiotic pathway by which IdrAB reduces IO_3^- to HIO, which abiotically disproportionates to I^- and IO_3^-[16,37]. In this model, cytochrome c peroxidase like proteins ($IdrP_1$ and $IdrP_2$) detoxify reactive H_2O_2 byproducts. Genes for this metabolism are part of a highly conserved IO_3^- reduction genomic island (IRI). Organisms harboring the IRI belong to phylogenetically distinct taxa, many of which are associated with marine sediments or multicellular hosts, suggesting that DIR is a horizontally transferred metabolism across marine ecosystems over geologic time. The abundance of IdrA genes across ocean metagenomes strongly correlates to oxygen minimum zones, indicating a niche for this metabolism in low-oxygen, high nitrate habitats across the ocean, from sediments to oxygen-minimum zones to the surfaces of multicellular organisms. In high-nitrate, low-oxygen conditions, bacteria with the IRI can use IO_3^- as an electron acceptor to obtain energy from the oxidation of organic matter. IO_3^- is constantly replenished by the chemical oxidation of I^-, so DIRM do not rely on other organisms for their substrate. IO_3^- is typically scarce (0.45µM in seawater)[4], so DIRM must compete with IO_3^- reduction by chemical reductants and by inadvertent biological activity, such as by algae, that contribute to the relative depletion of IO_3^- in those waters[7,61,65,69,70]. By analogy, perchlorate-reducing bacteria, which are common but sparse due to low natural abundance of perchlorate[71], may provide further insight into the ecology of DIRM broadly. The rarity of IO_3^- reduction genes among bacteria despite the ability of the metabolism to be horizontally transferred likely reflects the evolutionary constrains of growth by DIR. Intriguingly, one organism, *Sedimenticola thiotaurini*, seemingly possesses both perchlorate and IO_3^- reduction pathways, presenting future opportunities to study the ecology of these metabolically versatile

336 microorganisms[72]. Moreover, organisms such as *Vibrio spp.* and *Moritella spp.* show some degree
337 of vertical transfer for the IRI throughout recent evolutionary history, indicating possible niches
338 among sea fauna and cold environments where DIR is biogeochemically favorable. Future studies
339 addressing the affinity of IdrAB for IO_3^- may also shed light on how DIRM thrive at such low
340 environmental concentrations. Additionally, further research into the chemistry of iodine
341 oxyanions may provide insight on the intermediates of IO_3^- reduction. Addressing these open
342 questions may ultimately shed light on new potential niches for DIRM and provide a role for these
343 organisms in potentiating iodine redox cycling globally.

344

345 **Description and Phylogeny of *Denitromonas iodocrescerans* sp. nov. strain IR-12^T**

346 *Denitromonas iodocrescerans* (i.o.do.cre'scer.ans) Chem. n. *iodo* as it pertains to iodine; L. pres.
347 part. *crescerans* for growing; N.L. pres. part. *iodocrescerans* iodine-growing.

348 *D. iodocrescerans* is a facultatively anaerobic chemoorganotroph, gram negative, rod-shaped, 1.5-
349 2.0 µM long by 0.6-0.7 µM wide, and motile by means of a unipolar flagellum (Figure 1B).
350 Colonies are circular, smooth, and range in color from transparent to an opaque/whitish-sky blue
351 color after 48 hours of growth on R2A agar at 30°C. Extended growth on R2A agar (96 or more
352 hours) results in a light coral pink colony color. *D. iodocrescerans* grows by oxidizing D-glucose,
353 lactate, or acetate with concomitant reduction of oxygen (O_2), nitrate (NO_3^-), or iodate (IO_3^-). It
354 grows on up to 4 mM of iodate with an optimum at 2 mM. Additionally, the organism can tolerate
355 up to 6.25 mM of iodide. Growth occurs between 20-30°C with an optimum of 30°C. It grows at
356 a range of 0-5% salinity with an optimum of 3% NaCl on minimal media. *D. iodocrescerans* has
357 an innate resistance to tetracycline (10 µg/µL) and chloramphenicol (25 µg/µL) but is sensitive to
358 kanamycin, which inhibits growth at concentrations as low as 5 µg/µL.

359 The genome of *D. iodocrescerans* is 5,181,847 bp (average coverage 64.2x) with 4697 CDS, a
360 G+C content of 66.54%, 57 tRNAs, one tmRNA, one CRISPR, and a single plasmid 81,584 bp
361 long whose function remains unclear. The full genome has been deposited in GenBank (BioProject
362 ID PRJNA683738) currently consisting of 202 contigs. Phylogenetically, *D. iodocrescerans*
363 belongs to the class *Betaproteobacteria*; however, its phylogeny beyond this class becomes less
364 clear. The 16S rRNA locus suggests that *D. iodocrescerans* is a subclade of *Azoarcus*, which
365 belongs to the family *Zoogloeaceae*[73]. However, the NCBI database suggests that the genus
366 *Denitromonas* belongs to the family *Rhodocyclaceae*.

367 The type strain of *Denitromonas iodocrescerans*, IR-12^{T,} was enriched from marine sediment from
368 the Berkeley Marina in the San Francisco Bay during the Fall of 2018 (further details explained in
369 methods below). The strain has been deposited in the American Type Culture Collection (ATCC
370 XXXXX).

371

372 **Acknowledgements**

373 The authors acknowledge Mariana Shalit, Dylan Dang, Jessica Kretschmer, Rachael Peng,
374 Mitchell Thompson, and Hans Carlson for lab support and advice throughout the project. Funding

for research on iodate in the Coates lab was provided to VRU through the NSF GRFP Base Award: DGE1752814.

Conflict of Interest

The authors declare that they have no conflict of interest with the research presented in this article.

Contributions

JDC guided the research. VRU and KL performed all physiology experiments and measurements. VRU performed all cloning experiments. VRU and TPB performed the comparative genomic analysis and phylogenetic analyses. VRU and ZH performed the analysis of the TARA Oceans data. VRU and JDC developed the model. VRU wrote the draft manuscript and created the figures with guidance from JDC. All authors contributed to data analysis, reviewed the manuscript, and approved of its publication.

Methods

Media, chemicals, and culture conditions

Anaerobic enrichment cultures from marine environments were grown at 30°C using a minimal media containing the following per liter: 0.54g NH_4Cl, 0.14g KH_2PO_4, 0.20g $MgCl_2 \cdot 6\ H_2O$, 0.14g $Na_2SO_4 \cdot 10\ H_2O$, 20.0g NaCl, 0.24g Na_2MoO_4 0.20g, and 2.5g $NaHCO_3$ with an added vitamin mix and mineral mix. Oxygen was removed from the media and bottles were dispensed in an 80%N_2/20%CO_2 atmosphere. Anaerobic subcultures for isolation were grown in Artificial Pore Water (APM) medium at 30°C (30.8g NaCl, 1.0g NH_4Cl, 0.77g KCl, 0.1g KH_2PO_4, 0.20g MgSO4·7H2O, 0.02g $CaCl_2 \cdot 2\ H_2O$, 7.16g HEPES, along with vitamin and mineral mixes. A post sterile addition of 34.24mL 0.4M CaCl2 and 26.07mL 2M $MgCl_2 \cdot 6H_2O$ was added to all APM media. Conditions with lactate, acetate, iodate, and nitrate all used the sodium salts of these compounds. Conditions without molybdenum omitted Na_2MoO_4 from the mineral mixes. Aerobic cultures were all grown either on APM, R2A (HiMedia, USA), or R2A agar (BD Biosciences, USA). Kanamycin concentrations when used were at one tenth the standard concentrations on plates (5 mg/L, Sigma Aldrich, USA) and at one fourth the standard concentration in liquid (12.5 mg/L). All compounds were purchased through Sigma Aldrich (Sigma Aldrich, USA). Growth of tubes were measured either using the Thermo Scientific™ GENESYS™ 20 or the TECAN Sunrise™ 96-well microplate reader set at a wavelength of 600 nm. For growth measurements in Hungate tubes, a special adapter was built to measure the tubes on the GENESYS™ 20. Growth experiments using the microplate reader were run in an anerobic glove bag.

Isolation of dissimilatory iodate-reducing bacteria

Sediment from the oxic/anoxic boundary layer in the San Francisco Bay estuary (37°86'56.4" N, -122°30'63.9" W) was added to anaerobic media bottles at 25g/100mL for isolation of dissimilatory iodate-reducing bacteria. Samples were degassed and amended with acetate and iodate to enable growth of heterotrophic iodate reducing bacteria. Enrichments that showed iodate reduction to iodide were then passaged at least five times into fresh minimal media with 10mM acetate and 2mM iodate. To ensure purity of the passaged enrichment culture, the organism was plated aerobically onto an agar plate containing the minimal media, and a single colony was isolated from this plate.

Strains and plasmids

All plasmids, primers and strains constructed are listed in Table S1. The *E. coli* strain used for plasmid propagation was XL1-Blue, while WM3064 was used to perform conjugations. Plasmid pNTPS138, a generous gift from the Kathleen Ryan Lab at UC Berkeley, was used for the SacB counterselection. Plasmid pBBR1-MCS2 is a low copy expression vector and was used for complementation experiments. All expression plasmids and deletion vectors were constructed using the Benchling software suite (San Francisco, USA). Plasmids were assembled either by Gibson assembly or restriction digestion and ligation using standard procedures. Gibson assembly was carried out using NEB HiFi 2x Master Mix, and remaining enzymes and master mixes were ordered from New England Biosciences (NEB, USA). Plasmids were routinely isolated using the Qiaprep Spin Miniprep kit (Qiagen, USA), and all primers were ordered from Integrated DNA Technologies (IDT, Coralville, IA). Amplification of DNA for generating assembly products was performed using Q5 DNA Polymerase 2x Master Mix (NEB, USA) with 3% DMSO. Amplification of distinct portions of the genome were optimized since most sequences in the iodate reduction cluster contain at minimum 60% GC content, making amplification relatively challenging. All *D. iodocrescerans* strains (pre- or post-transformation) were propagated from glycerol stocks (25% glycerol) stored at -80°C, grown on a plate for up to 72 hours, picked and then grown for an additional 48-72 hours in liquid R2A. For additional information on performing transformations and conjugations in *D. iodocrescerans* see supplemental methods.

Iodate and iodide quantification

A Dionex™ IonPac™ AS25 Anion Exchange Column (Thermo Fischer, USA) was used exclusively to measure the consumption of iodate and acetate, as well as the production of iodide in all samples. Briefly, all samples are diluted 1:25 in deionized water and loaded onto the autosampler for processing. Standards are made by serial dilution starting with 1 mM of the standard molecule. All samples were run in triplicate. Acetate peaks were consistently detected at 3.6 minutes, iodate peaks were consistently detected at 3.8 minutes, and iodide peaks were consistently detected at 11.5 minutes at a flow rate of 1mL/min.

Genome sequencing, comparative genomics, and phylogenetic analysis

Genome sequencing was carried out on an Illumina HiSeq4000 using 150bp paired end reads. The genome was subsequently assembled using SPAdes 3.9[74] and the assembly graph was assessed for completion using bandage[75]. The Prokka (version 1.14) pipeline was then used to generate the genome annotations and the general feature format file (.gff), which allowed for genome navigation and visualization on the Artemis software (available at http://sanger-

pathogens.github.io)[76]. To search for the iodate reduction island, MMseqs2 was used to cluster homologous proteins in the amino acid FASTA (.faa) files from *D. iodocrescerans*, *P. stutzeri* sp. SCT, *D. halophilus* SFB-1, and *P. stutzeri* sp. CAL by subfamily[41]. A presence and absence matrix for each subfamily was generated and represented as a four-way Venn diagram using pyvenn (https://github.com/tctianchi/pyvenn). To identify additional iodate reductase proteins in public databases, a profile-HMM was constructed using HMMER 3.0 following a multiple sequence alignment using MUSCLE 3.8 on the molybdopterin oxidoreductase (Pfam_00384) seed set and *D.* iodocrescerans/*P. stutzeri* SCT IdrA proteins[77,78]. A separate arsenite oxidase (AioA) profile-HMM was created using analogous methods. Genomes from high probability HMM hits (threshold above 640 on https://www.ebi.ac.uk/Tools/hmmer/search/phmmer) and BLAST hits were downloaded from NCBI using ncbi-genome-download (https://github.com/kblin/ncbi-genome-download). Approximately-maximum-likelihood phylogenetic trees were generated using Fasttree[79] specifying 10,000 resamples and using standard settings for everything else. Visualization of resultant trees used the ete3 toolkit[80]. To perform the neighborhood frequency analysis, 10 genes upstream and downstream from the *aioA* or *idrA* locus were extracted from the associated GenBank files for each genome, and MMseqs2 was used to cluster homologous proteins into subfamilies [41]. To search for cld in the downloaded genomes, a profile-HMM for cld, described previously, was used[81]. Frequency was calculated as number of genomes in possession of a cluster divided by the total number of genomes. Projections of this data were drawn using a custom Python 3.7 script. All tanglegram analyses used Dendroscope to load trees for processing and visualization[47].

Distribution of iodate reductase in ocean metagenomes

The profile-HMM for iodate reductase (described above) was used to search all 40 million non-redundant open reading frames from the 243-sample Tara oceans dataset. Open reading frames were downloaded (available from https://www.ebi.ac.uk/ena/data/view/PRJEB7988) and translated to amino acid sequences using custom BioPython code[82,83,84]. The amino acid sequences in the 0.22-micron and 0.45-micron range were then searched for hits using the IdrA profile-HMM set at a threshold score of 640. Hits were then grouped by station for further analysis. Reads were mapped to scaffolds with Bowtie2[85] and reads were counted using SAMtools[86]. Read abundance mapping to these unique IdrA hits were quantified by using the transcripts per million (TPM) method for read quantification as described in Ribicic *et al*[58,59]. Ten variables in the metadata associated with the chemical environment at each sampling location were analyzed using the principal component analysis module on scikit-learn 0.23.1[87]. All sites regardless of *idrA* presence were included in the analysis. Missing metadata values were imputed using the Multivariate Imputation by Chained Equations method (MICE)[88]. Variables included in the analysis were 'Sampling depth [m]', 'Mean_Temperature [deg C]', 'Mean_Salinity [PSU]','Mean_Oxygen [umol/kg]', 'Mean_Nitrates[umol/L]', 'NO2 [umol/L]', 'PO4 [umol/L]', 'SI [umol/L]','NO2NO3 [umol/L]', and irradiance 'AMODIS:PAR8d,Einsteins/m-2/d-1'. Components were built using "pca.fit_transform()" and confidence ellipses at one standard deviation were set for each group. Component coefficients were extracted from principal components by using "pca.components_" and displayed as a loadings plot. Explained variance was also extracted from "pca.components_" to display on PCA axes. The map of *idrA* abundance was created using Cartopy 0.17.

Figure legends.

Figure 1: Phylogeny and Physiology of *Denitromonas iodocrescerans.* A) 16S rRNA gene phylogeny of *Denitromonas iodocrescerans* (denoted by a purple star) belonging to a subclade of *Azoarcus*, separate from other known *Azoarcus* species. B) TEM images of an active culture of *D. iodocrescerans* with the scale at 2 μm (left) and 0.2 μm (right) taken on a Technai 12 TEM. C) Iodate consumption (■), acetate consumption (▲), iodide production (■), and growth (●; measured as optical density at λ=600nm; OD600) in an active culture of *D. iodocrescerans* growing anaerobically. N=3 and error bars show standard deviation. D) Iodate consumption across all five conditions assessed in the growth experiment in C. N=3 and error bars show standard deviation. E) Optical density (OD600) in the presence (■),absence (●), and amendment after 14 hours incubation (▲) of MoO_4^{2-}. N=7 and error bars show standard deviation.

Figure 2: Identification of unique gene cluster in iodate reducing genomes enablling the identification and characterization of the iodate reductase (IdrA). A) A four-way comparison between two genomes from confirmed DIRM (solid line) and two genomes from closely related non-DIRM (dotted line) identifying 26 shared genes among the two taxonomically distinct iodate reducing bacteria (Table S2). B) The three genes upstream of the predicted molybdopterin oxidoreductase (IdrA) involved in DIR. C) anaerobic growth of wildtype of *D. iodocrescerans* in the presence (●) or absence (●) of iodate in comparison to the Δ*idrA mutant* (⬟) or the Δ*idrA* mutant complemented with an empty vector (▲) or with *idrA* in *trans* (■). N=8 and error bars represent standard deviation.

F**igure 3** Mechanistic and Ecological Models of Iodate Reduction. A) A representation of the electron flow (black arrows) from the quinone pool to iodate in *D. iodocrescerans*. Abbreviations: QH_2—reduced quinone, Q—oxidized quinone, bc1—bc1 complex, IO_3^-iodate, HIO—hypoiodous acid, I^-iodide. Gray arrows represent micromolar production of yet unknown oxidant that is detoxified by $IdrP_1$ and $IdrP_2$. B) Ecological model of iodate reducing bacteria. Top right panel represents locations in the open ocean near oxygen minimum zones inhabited by DIORM. Bottom right panel represents host associated DIORM. DOM—dissolved organic matter.

Figure 4 Phylogeny and Taxonomic Distribution of IdrA. A) Phylogeny of Molybdopterin Oxidoreductases (Pfam 00384) using pre-aligned proteins from the representative proteomes 55 dataset. Green bars indicate location of an individual protein in each branch belonging to the labelled group. B) Phylogeny of IdrA (purple), AioA (gray), and an unknown clade (light green) that contains proteins from organisms showing demonstrated arsenite oxidation abilities. Colored circles along the edges of the IdrA clade indicate the different Phyla each organism belongs to.

Figure 5 Phylogeny and Gene Neighborhoods of arsenite oxidase, iodate reductase, and the associated unknown clade. A pruned tree of the molybdopterin oxidoreductase phylogeny (left) showing a representative subset of genomes identified from Figure 3B. *Denitromonas iodocrescerans* is illustrated in bold. Genome neighborhoods (right) show 10 genes upstream and downstream (if present) from the *idrA* locus. Individual genes were clustered into groups based on amino acid similarity using MMSeqs2 and the frequency of genomes possessing an individual cluster is colored by the intensity of purple. Circles above each gene represents either the

molybdopterin oxidoreductase (●), the associated Rieske containing subunit (●), or the di-haem cytochrome c peroxidases (●).

Figure 6 Analysis of Tara Oceans dataset identifies possible ecological niche above oxygen minimum zones. A) A map indicating sampled locations during the Tara expedition (x) alongside sampling locations with IdrA present (purple circles). Markers overlaid directly on top of each other demonstrate transect samples from different depths at a given location. Size of purple circle shows the cumulative TPM at a particular site. B) Chart on the left shows the TPM of individual hits on a scaffold organized by Tara location identifier. Coloration represents the individual Tara station while marker shape indicates general geographic location. Chart on the right correlates the number of unique IdrA hits at any given site to the cumulative TPM at an individual location. Tara station is denoted by color and general geographic location is denoted by marker shape. C) A principal component analysis displaying the first two principal components. Locations are grouped by IdrA absent (x), presence of a single IdrA hit (■), or presence of multiple hits (■). Ellipses represent 1 standard deviation of the mean. The color of the ellipse corresponds to the variable grouping. D) A loading plot of the ten variables used in the first two principal components with variables identified at the end of each arrow. E) The means of select environmental variables at IdrA present sites (purple) and IdrA absent sites (gray). Error bars indicate 95% confidence interval. Units for each of the variables are located near the variable name.

References

1 Carpenter, L. J. in *Encyclopedia of Atmospheric Sciences* 205-219 (Elsevier, 2015).

2 Chemburkar, S. R., Deming, K. C. & Reddy, R. E. Chemistry of thyroxine: an historical perspective and recent progress on its synthesis. *Tetrahedron* **66**, 1955-1962, doi:10.1016/J.TET.2009.12.044 (2010).

3 Schweizer, U. & Steegborn, C. Thyroid hormones—From crystal packing to activity to reactivity. *Angew. Chem* **54**, 12856-12858, doi:10.1002/anie.201506919 (2015).

4 Küpper, F. C. *et al.* Commemorating two centuries of iodine research: an interdisciplinary overview of current research. *Angew. Chem* **50**, 11598-11620, doi:10.1002/anie.201100028 (2011).

5 Manley, S. L. & Dastoor, M. N. Methyl iodide (CH3I) production by kelp and associated microbes. *Marine Biol* **98**, 477-482, doi:10.1007/BF00391538 (1988).

6 Lebel, L. S., Dickson, R. S. & Glowa, G. A. Radioiodine in the atmosphere after the Fukushima Dai-ichi nuclear accident. *J Environ Radioact* **151**, 82-93, doi:10.1016/j.jenvrad.2015.06.001 (2016).

7 Luther, G. W., Wu, J. & Cullen, J. B. Redox Chemistry of Iodine in Seawater Frontier Molecular Orbital Theory Considerations. *Aquat Chem Adv*, doi:10.1021/ba-1995-0244.ch006 (1995).

8 Gonzales, J., Tymon, T., Küpper, F. C., Edwards, M. S. & Carrano, C. J. The potential role of kelp forests on iodine speciation in coastal seawater. *PLOS ONE* **12**, e0180755, doi:10.1371/journal.pone.0180755 (2017).

9 Tsunogai, S. & Sase, T. Formation of iodide-iodine in the ocean. *Deep Sea Research and Oceanographic Abstracts* **16**, 489-496, doi:10.1016/0011-7471(69)90037-0 (1969).

10 Councell, T. B., Landa, E. R. & Lovley, D. R. Microbial reduction of iodate. *Wat Air Soil Pollut* **100**, 99–106. https://doi.org/10.1023/A (1997)

11 Youngblut, M. D. *et al.* Perchlorate Reductase Is Distinguished by Active Site Aromatic Gate Residues. *J Biol Chem* **291**, 9190-9202, doi:10.1074/jbc.M116.714618 (2016).

12 Farrenkopf Ay, A. M. *et al.* Reduction of iodate in seawater during Arabian Sea incubations and in laboratory cultures of the marine *Shewanella putrefaciens* strain MR-4 shipboard bacterium. *Marine Chem* **57**, 347-354 (1997).

13 Amachi, S. *et al.* Dissimilatory iodate reduction by marine Pseudomonas sp. strain SCT. *Appl Environ Microbiol* **73**, 5725-5730, doi:10.1128/AEM.00241-07 (2007).

14 Yamazaki, C. *et al.* A novel dimethylsulfoxide reductase family of molybdenum enzyme, Idr, is involved in iodate respiration by *Pseudomonas* sp. SCT. *Environ Microbiol* **n/a**, doi:10.1111/1462-2920.14988 (2020).

15 Youngblut, M. D., Wang, O., Barnum, T. P. & Coates, J. D. (Per)chlorate in biology on earth and beyond. *Ann rev Microbiol* **70**, 435-457, doi:10.1146/annurev-micro-102215-095406 (2016).

16 WHO. Alternative drinking-water disinfectants. 52-55 (2018).

17 Haimovich, O. & Treinin, A. Disproportionation of hypoiodite. *J Phys Chem* **71**, 1941-1943, doi:10.1021/j100865a068 (1967).

18 Toporek, Y. J. *et al.* Metal reduction and protein secretion genes required for iodate reduction by *Shewanella oneidensis*. *Appl Environ Microbiol* **85**, doi:10.1128/aem.02115-18 (2019).

19 Carlström, C. I. *et al.* Characterization of an anaerobic marine microbial community exposed to combined fluxes of perchlorate and salinity. *Appl Microbiol Biotechnol* **100**, 9719-9732, doi:10.1007/s00253-016-7780-5 (2016).

20 Yip, K. C.-W. & Gu, J.-D. A novel bacterium involved in the degradation of 2-methylindole isolated from sediment of Inner Deep Bay of Hong Kong. *Appl Environ Biotechnol* **1**, 52-63 (2015).

21 Glazyrina, J. *et al.* High cell density cultivation and recombinant protein production with *Escherichia coli* in a rocking-motion-type bioreactor. *Microb Cell Fact* **9**, 42, doi:10.1186/1475-2859-9-42 (2010).

22 Loferer-Krössbacher, M., Klima, J. & Psenner, R. Determination of bacterial cell dry mass by transmission electron microscopy and densitometric image analysis. *Appl Environ Microbiol* **64**, 688-694, doi:10.1128/aem.64.2.688-694.1998 (1998).

23 McInerney, M. J. & Beaty, P. S. Anaerobic community structure from a nonequilibrium thermodynamic perspective. *Can J Microbiol* **34**, 487-493, doi:10.1139/m88-083 (1988).

24 Stern, J. H. & Passchier, A. A. The heats of formation of triiodide and iodate ions. *J Phys Chem* **66**, 752-753, doi:10.1021/j100810a041 (1962).

25 Weber, K. A., Achenbach, L. A. & Coates, J. D. Microorganisms pumping iron: anaerobic microbial iron oxidation and reduction. *Nat Rev Microbiol* **4**, 752-764, doi:10.1038/nrmicro1490 (2006).

26 Leimkühler, S. & Iobbi-Nivol, C. Bacterial molybdoenzymes: old enzymes for new purposes. *FEMS Microbiol Rev* **40**, 1-18, doi:10.1093/femsre/fuv043 (2016).

27 McEwan, A. G., Ridge, J. P., McDevitt, C. A. & Hugenholtz, P. The DMSO reductase family of microbial molybdenum enzymes; molecular properties and role in the dissimilatory reduction of toxic elements. *Geomicrobiol J* **19**, 3-21, doi:10.1080/01490450231724613 8 (2002).

28 Chaudhuri, S. K., O'Connor, S. M., Gustavson, R. L., Achenbach, L. A. & Coates, J. D. Environmental factors that control microbial perchlorate reduction. *Appl Environ Microbiol* **68**, 4425-4430, doi:10.1128/aem.68.9.4425-4430.2002 (2002).

29 Snel, B., Bork, P. & Huynen, M. A. Genomes in flux: the evolution of archaeal and proteobacterial gene content. *Gen Res* **12**, 17-25 (2002).

30 Saunders, J. K., Fuchsman, C. A., McKay, C. & Rocap, G. Complete arsenic-based respiratory cycle in the marine microbial communities of pelagic oxygen-deficient zones. *Proc Nat Acad Sci*, 201818349, doi:10.1073/pnas.1818349116 (2019).

31 Dabir, D. V. *et al.* A role for cytochrome c and cytochrome c peroxidase in electron shuttling from Erv1. *EMBO J* **26**, 4801-4811 (2007).

32 Martins, D., Kathiresan, M. & English, A. M. Cytochrome c peroxidase is a mitochondrial heme-based H2O2 sensor that modulates antioxidant defense. *Free Rad Bio Med* **65**, 541-551 (2013).

33 Almagro Armenteros, J. J. *et al.* SignalP 5.0 improves signal peptide predictions using deep neural networks. *Nat Biotechnol* **37**, 420-423, doi:10.1038/s41587-019-0036-z (2019).

34 Berks, B. C. The Twin-Arginine Protein Translocation Pathway. *Annl Rev Biochem* **84**, 843-864, doi:10.1146/annurev-biochem-060614-034251 (2015).

35 Toporek, M., Michałowska-Kaczmarczyk, A. M. & Michałowski, T. Disproportionation reactions of HIO and NaIO in static and dynamic systems. *Am J Anal Chem* **5**, 1046 (2014).

36 Youngblut, M. D. *et al.* Perchlorate reductase is distinguished by active site aromatic gate residues. *J Biol Chem* **291**, 9190-9202, doi:10.1074/jbc.M116.714618 (2016).

37 Ellis, K. V. & Van Vree, H. B. R. J. Iodine used as a water-disinfectant in turbid waters. *Wat Res* **23**, 671-676, doi:https://doi.org/10.1016/0043-1354(89)90198-X (1989).

38 Liebensteiner, M. G., Pinkse, M. W. H., Schaap, P. J., Stams, A. J. M. & Lomans, B. P. Archaeal (per) chlorate reduction at high temperature: an interplay of biotic and abiotic reactions. *Science* **340**, 85-87 (2013).

39 Dudley, M., Salamone, A. & Nerenberg, R. Kinetics of a chlorate-accumulating, perchlorate-reducing bacterium. *Wat Res* **42**, 2403-2410, doi:https://doi.org/10.1016/j.watres.2008.01.009 (2008).

40 Melnyk, R. A. *et al.* Novel mechanism for scavenging of hypochlorite involving a periplasmic methionine-rich peptide and methionine sulfoxide reductase. *MBio* **6** (2015).

41 Steinegger, M. & Söding, J. MMseqs2 enables sensitive protein sequence searching for the analysis of massive data sets. *Nat Biotechnol* **35**, 1026-1028, doi:10.1038/nbt.3988 (2017).

42 Ordoñez, O. F., Rasuk, M. C., Soria, M. N., Contreras, M. & Farías, M. E. *Haloarchaea* from the Andean Puna: biological role in the energy metabolism of arsenic. *Microb Ecol* **76**, 695-705, doi:10.1007/s00248-018-1159-3 (2018).

43 Anantharaman, K. *et al.* Thousands of microbial genomes shed light on interconnected biogeochemical processes in an aquifer system. *Nat Comm* **7**, 13219, doi:10.1038/ncomms13219 (2016).

44 Becraft, E. D. *et al.* Rokubacteria: Genomic giants among the uncultured bacterial phyla. *Front Microbiol* **8**, doi:10.3389/fmicb.2017.02264 (2017).

45 He, Z. *et al.* A novel denitrifying methanotroph of the NC10 phylum and its microcolony. *Sci Rep* **6**, 32241, doi:10.1038/srep32241 (2016).

46 Melnyk, R. A. *et al.* Identification of a perchlorate reduction genomic island with novel regulatory and metabolic genes. *Appl Environ Microbiol* **77**, 7401-7404, doi:10.1128/AEM.05758-11 (2011).

47 Scornavacca, C., Zickmann, F. & Huson, D. H. Tanglegrams for rooted phylogenetic trees and networks. *Bioinformatics (Oxford, England)* **27**, i248-i256, doi:10.1093/bioinformatics/btr210 (2011).

48 Juhas, M. *et al.* Genomic islands: tools of bacterial horizontal gene transfer and evolution. *FEMS Microbiol Rev* **33**, 376-393, doi:10.1111/j.1574-6976.2008.00136.x (2009).

49 Reiter, W. D., Palm, P. & Yeats, S. Transfer RNA genes frequently serve as integration sites for prokaryotic genetic elements. *Nucl Acid Res* **17**, 1907-1914, doi:10.1093/nar/17.5.1907 (1989).

50 Larbig, K. D. *et al.* Gene islands integrated into tRNAGly genes confer genome diversity on a *Pseudomonas aeruginosa* clone. *J Bacteriol* **184**, 6665, doi:10.1128/JB.184.23.6665-6680.2002 (2002).

51 Boyd, E. & Barkay, T. The mercury resistance operon: from an origin in a geothermal environment to an efficient detoxification machine. *Front Microbiol* **3**, doi:10.3389/fmicb.2012.00349 (2012).

52 Besaury, L. *et al.* Abundance and diversity of copper resistance genes cusA and copA in microbial communities in relation to the impact of copper on Chilean marine sediments. *Mar Pollut Bull* **67**, 16-25, doi:https://doi.org/10.1016/j.marpolbul.2012.12.007 (2013).

53 Jin, H. M. *et al. Litorimicrobium taeanense* gen. nov., sp. nov., isolated from a sandy beach. *International J Sys Evol Microbiol* **61**, 1392-1396, doi:https://doi.org/10.1099/ijs.0.025007-0 (2011).

54 Alex, A. & Antunes, A. Comparative genomics reveals metabolic specificity of *Endozoicomonas* isolated from a marine sponge and the genomic repertoire for host-bacteria symbioses. *Microorganisms* **7**, 635 (2019).

55 Kim, Y.-O. *et al. Litoreibacterascidiaceicola* sp. nov., isolated from the golden sea squirt *Halocynthiaaurantium*. *Int J Sys Evol Microbiol* **64**, 2545-2550, doi:https://doi.org/10.1099/ijs.0.064196-0 (2014).

56 Kupper, F. C. *et al.* Iodide accumulation provides kelp with an inorganic antioxidant impacting atmospheric chemistry. *Proc Nat Acad Sci* **105**, 6954-6958, doi:10.1073/pnas.0709959105 (2008).

57 Jung, H. S., Jeong, S. E., Chun, B. H., Quan, Z.-X. & Jeon, C. O. *Rhodophyticola porphyridii* gen. nov., sp. nov., isolated from a red alga, *Porphyridium marinum*. *Int J Sys Evol Microbiol* **69**, 1656-1661, doi:https://doi.org/10.1099/ijsem.0.003371 (2019).

58 Wagner, G. P., Kin, K. & Lynch, V. J. Measurement of mRNA abundance using RNA-seq data: RPKM measure is inconsistent among samples. *Theory Biosci* **131**, 281-285, doi:10.1007/s12064-012-0162-3 (2012).

59 Ribicic, D. *et al.* Microbial community and metagenome dynamics during biodegradation of dispersed oil reveals potential key-players in cold Norwegian seawater. *Mar Pollut Bull* **129**, 370-378, doi:https://doi.org/10.1016/j.marpolbul.2018.02.034 (2018).

60 Lachkar, Z., Lévy, M. & Smith, K. S. Strong intensification of the Arabian Sea oxygen minimum zone in response to Arabian Gulf warming. *Geophys Res Lett* **46**, 5420-5429, doi:10.1029/2018gl081631 (2019).

61 Farrenkopf, A. M. & Iii, G. W. L. Iodine chemistry reflects productivity and denitrification in the Arabian Sea: evidence for flux of dissolved species from sediments of western India into the OMZ. *Deep-Sea Res II* **49**, 2303-2318 (2002).

62 Bertagnolli, A. D. & Stewart, F. J. Microbial niches in marine oxygen minimum zones. *Nat Rev Microbiol* **16**, 723-729, doi:10.1038/s41579-018-0087-z (2018).

63 Cutter, G. A., Moffett, J. W., Nielsdóttir, M. C. & Sanial, V. Multiple oxidation state trace elements in suboxic waters off Peru: In situ redox processes and advective/diffusive horizontal transport. *Mar Chem* **201**, 77-89, doi:10.1016/J.MARCHEM.2018.01.003 (2018).

64 Karstensen, J., Stramma, L. & Visbeck, M. Oxygen minimum zones in the eastern tropical Atlantic and Pacific oceans. *Prog Ocean* **77**, 331-350, doi:https://doi.org/10.1016/j.pocean.2007.05.009 (2008).

65 Farrenkopf, A. M., Luther, G. W., Truesdale, V. W. & Van Der Weijden, C. H. Sub-surface iodide maxima: evidence for biologically catalyzed redox cycling in Arabian Sea OMZ during the SW intermonsoon. *Deep Sea Res Part II: Topical Studies in Oceanography* **44**, 1391-1409, doi:https://doi.org/10.1016/S0967-0645(97)00013-1 (1997).

66 Kalvelage, T. *et al.* Aerobic microbial respiration in oceanic oxygen minimum zones. *PloS one* **10**, e0133526-e0133526, doi:10.1371/journal.pone.0133526 (2015).

67 Howarth, R. W. Nutrient limitation of net primary production in marine ecosystems. *Ann Rev Ecol Sys* **19**, 89-110 (1988).

68 Shalel Levanon, S., San, K.-Y. & Bennett, G. N. Effect of oxygen on the *Escherichia coli* ArcA and FNR regulation systems and metabolic responses. *Biotech Bioeng* **89**, 556-564, doi:10.1002/bit.20381 (2005).

69 Wadley, M. R. *et al. Modelling iodine in the ocean*. (2020).

70 Waite, T. J. & Truesdale, V. W. Iodate reduction by *Isochrysis galbana* is relatively insensitive to de-activation of nitrate reductase activity—are phytoplankton really responsible for iodate reduction in seawater? *Mar Chem* **81**, 137-148, doi:10.1016/S0304-4203(03)00013-6 (2003).

71 Coates, J. D. & Achenbach, L. A. Microbial perchlorate reduction: rocket-fuelled metabolism. *Nat Rev Microbiol* **2**, 569-580, doi:10.1038/nrmicro926 (2004).

72 Jones, D. S., Bailey, J. V. & Flood, B. E. *Sedimenticola thiotaurini* sp. nov., a sulfur-oxidizing bacterium isolated from salt marsh sediments, and emended descriptions of the genus

Sedimenticola and *Sedimenticola selenatireducens*. *Int J Sys Evol Microbiol* **65**, 2522-2530, doi:10.1099/ijs.0.000295 (2015).

73 Boden, R., Hutt, L. P. & Rae, A. W. Reclassification of *Thiobacillus aquaesulis* (Wood & Kelly, 1995) as *Annwoodia aquaesulis* gen. nov., comb. nov., transfer of *Thiobacillus* (Beijerinck, 1904) from the *Hydrogenophilales* to the *Nitrosomonadales*, proposal of *Hydrogenophilalia* class. nov. within the 'Proteobacteria', and four new families within the orders *Nitrosomonadales* and *Rhodocyclales*. *Int J Sys Evol Microbiol* **67**, 1191-1205, doi:https://doi.org/10.1099/ijsem.0.001927 (2017).

74 Bankevich, A. *et al.* SPAdes: a new genome assembly algorithm and its applications to single-cell sequencing. *J Comput Biol* **19**, 455-477, doi:10.1089/cmb.2012.0021 (2012).

75 Wick, R. R., Schultz, M. B., Zobel, J. & Holt, K. E. Bandage: interactive visualization of de novo genome assemblies. *Bioinformatics* **31**, 3350-3352, doi:10.1093/bioinformatics/btv383 (2015).

76 Seemann, T. Prokka: rapid prokaryotic genome annotation. *Bioinformatics* **30**, 2068-2069, doi:10.1093/bioinformatics/btu153 (2014).

77 Eddy, S. HMMER user's guide. *Department of Genetics, Washington University School of Medicine* **2**, 13 (1992).

78 Edgar, R. C. MUSCLE: multiple sequence alignment with high accuracy and high throughput. *Nucl Acid Res* **32**, 1792-1797, doi:10.1093/nar/gkh340 (2004).

79 Price, M. N., Dehal, P. S. & Arkin, A. P. FastTree 2--approximately maximum-likelihood trees for large alignments. *PLoS One* **5**, e9490, doi:10.1371/journal.pone.0009490 (2010).

80 Huerta-Cepas, J., Serra, F. & Bork, P. ETE 3: Reconstruction, Analysis, and Visualization of Phylogenomic Data. *Mol Biol Evol* **33**, 1635-1638, doi:10.1093/molbev/msw046 (2016).

81 Barnum, T. P. *et al.* Genome-resolved metagenomics identifies genetic mobility, metabolic interactions, and unexpected diversity in perchlorate-reducing communities. *ISME J* **12**, 1568-1581, doi:10.1038/s41396-018-0081-5 (2018).

82 Cock, P. J. *et al.* Biopython: freely available Python tools for computational molecular biology and bioinformatics. *Bioinformatics* **25**, 1422-1423 (2009).

83 Karsenti, E. The making of Tara Oceans: funding blue skies research for our Blue Planet. *Mol Sys Biol* **11**, 811, doi:10.15252/msb.20156271 (2015).

84 Pesant, S. *et al.* Open science resources for the discovery and analysis of Tara Oceans data. *Sci Data* **2**, 150023, doi:10.1038/sdata.2015.23 (2015).

85 Langmead, B. & Salzberg, S. L. Fast gapped-read alignment with Bowtie 2. *Nat Meth* **9**, 357 (2012).

86 Li, H. *et al.* The sequence alignment/map format and SAMtools. *Bioinformatics* **25**, 2078-2079 (2009).

87 Pedregosa, F. *et al.* Scikit-learn: Machine learning in Python. *J Mach Learn Res* **12**, 2825-2830 (2011).

88 Azur, M. J., Stuart, E. A., Frangakis, C. & Leaf, P. J. Multiple imputation by chained equations: what is it and how does it work? *Int J Methods Psychiatr Res* **20**, 40-49, doi:10.1002/mpr.329 (2011).

89 Chao, L. S.-L., Davis, R. E. & Moyer, C. L. Characterization of bacterial community structure in vestimentiferan tubeworm Ridgeia piscesae trophosomes. *Mar Ecol* **28**, 72-85, doi:https://doi.org/10.1111/j.1439-0485.2007.00151.x (2007).

90 Patra, A. K. *et al.* Phylogenetic relationship between symbionts of tubeworm Lamellibrachia satsuma and the sediment microbial community in Kagoshima Bay. *Ocean Sci J* **51**, 317-332, doi:10.1007/s12601-016-0028-6 (2016).

91 Gardebrecht, A. *et al.* Physiological homogeneity among the endosymbionts of *Riftia pachyptila* and *Tevnia jerichonana* revealed by proteogenomics. *ISME J* **6**, 766-776, doi:10.1038/ismej.2011.137 (2012).

92 Wang, Z. *et al. Alginatibacterium sediminis* gen. nov., sp. nov., a novel marine gammaproteobacterium isolated from coastal sediment. *Int J Sys Evol Microbiol* **69**, 511-516, doi:https://doi.org/10.1099/ijsem.0.003187 (2019).

93 Park, S., Park, J.-M., Kang, C.-H. & Yoon, J.-H. *Aliiroseovarius pelagivivens* gen. nov., sp. nov., isolated from seawater, and reclassification of three species of the genus *Roseovarius* as *Aliiroseovarius crassostreae* comb. nov., *Aliiroseovarius halocynthiae* comb. nov. and *Aliiroseovarius sediminilitoris* comb. nov. *Int J Sys Evol Microbiol* **65**, 2646-2652, doi:https://doi.org/10.1099/ijs.0.000315 (2015).

94 Kasai, Y., Takahata, Y., Manefield, M. & Watanabe, K. RNA-based stable isotope probing and isolation of anaerobic benzene-degrading bacteria from gasoline-contaminated groundwater. *Appl Environ Microbiol* **72**, 3586-3592, doi:10.1128/aem.72.5.3586-3592.2006 (2006).

95 Jung, Y.-T., Park, S., Lee, J.-S. & Yoon, J.-H. *Defluviimonas aquaemixtae* sp. nov., isolated from the junction between a freshwater spring and the ocean. *Int J Sys Evol Microbiol* **64**, 4191-4197, doi:https://doi.org/10.1099/ijs.0.068767-0 (2014).

96 Zhang, D.-C. *et al. Marinobacter psychrophilus* sp. nov., a psychrophilic bacterium isolated from the Arctic. *Int J Sys Evol Microbiol* **58**, 1463-1466, doi:https://doi.org/10.1099/ijs.0.65690-0 (2008).

97 Kim, H. J. *et al. Moritella dasanensis* sp. nov., a psychrophilic bacterium isolated from the Arctic ocean. *Int J Sys Evol Microbiol* **58**, 817-820, doi:https://doi.org/10.1099/ijs.0.65501-0 (2008).

98 Nogi, Y. & Kato, C. Taxonomic studies of extremely barophilic bacteria isolated from the Mariana Trench and description of *Moritella yayanosii* sp. nov., a new barophilic bacterial isolate. *Extremophiles* **3**, 71-77, doi:10.1007/s007920050101 (1999).

99 Hameed, A. *et al. Oricola cellulosilytica* gen. nov., sp. nov., a cellulose-degrading bacterium of the family *Phyllobacteriaceae* isolated from surface seashore water, and emended descriptions of

Mesorhizobium loti and *Phyllobacteriummyrsinacearum. Antonie van Leeuwenhoek* **107**, 759-771, doi:10.1007/s10482-014-0370-6 (2015).

100 Hahnke, S., Tindall, B. J., Schumann, P., Simon, M. & Brinkhoff, T. *Pelagimonas varians* gen. nov., sp. nov., isolated from the southern North Sea. *Int J Sys Evol Microbiol* **63**, 835-843, doi:https://doi.org/10.1099/ijs.0.040675-0 (2013).

101 Li, Y. *et al. Photobacterium proteolyticum* sp. nov., a protease-producing bacterium isolated from ocean sediments of Laizhou Bay. *Int J Sys Evol Microbiol* **67**, 1835-1840, doi:https://doi.org/10.1099/ijsem.0.001873 (2017).

102 Rajasabapathy, R. *et al. Roseovarius azorensis* sp. nov., isolated from seawater at Espalamaca, Azores. *Antonie van Leeuwenhoek* **105**, 571-578, doi:10.1007/s10482-013-0109-9 (2014).

103 Pujalte, M. J., Macián, M. C., Arahal, D. R. & Garay, E. *Stappia alba* sp. nov., isolated from Mediterranean oysters. *Syst Appl Microbiol* **28**, 672-678, doi:10.1016/j.syapm.2005.05.010 (2005).

104 Colquhoun, D., Hovland, H., Hellberg, H., Haug, T. & Nilsen, H. *Moritella viscosa* isolated from farmed Atlantic cod (Gadus morhua). *Bull Eur Assoc Fish Path* **24**, 109-114 (2004).

105 Huang, Z., Guo, F., Lai, Q. & Shao, Z. *Notoacmeibacter marinus* gen. nov., sp. nov., isolated from the gut of a limpet and proposal of *Notoacmeibacteraceae* fam. nov. in the order Rhizobiales of the class Alphaproteobacteria. *Int J Sys Evol Microbiol* **67**, 2527-2531, doi:https://doi.org/10.1099/ijsem.0.001951 (2017).

106 Yan, X.-R. & Tuo, L. *Notoacmeibacter ruber* sp. nov., a novel endophytic bacterium isolated from leaf of *Rhizophora stylosa*. *Antonie van Leeuwenhoek* **112**, 919-925, doi:10.1007/s10482-019-01225-3 (2019).

107 O'Halloran, J. A. *et al. Pseudovibrio axinellae* sp. nov., isolated from an Irish marine sponge. *Int J Sys Evol Microbiol* **63**, 141-145, doi:https://doi.org/10.1099/ijs.0.040196-0 (2013).

108 Shiba, T. *Roseobacter litoralis* gen. nov., sp. nov., and *Roseobacter denitrificans* sp. nov., aerobic pink-pigmented bacteria which contain bacteriochlorophyll a. *Sys Appl Microbiol* **14**, 140-145, doi:https://doi.org/10.1016/S0723-2020(11)80292-4 (1991).

109 Kim, Y.-O. *et al. Ruegeria halocynthiae* sp. nov., isolated from the sea squirt *Halocynthia roretzi*. *Int J Sys Evol Microbiol* **62**, 925-930, doi:https://doi.org/10.1099/ijs.0.031609-0 (2012).

110 Flood, B. E. *et al.* Single-cell (meta-)genomics of a dimorphic candidatus *Thiomargarita nelsonii* reveals genomic plasticity. *Front Microbiol* **7**, doi:10.3389/fmicb.2016.00603 (2016).

111 Beaz-Hidalgo, R., Doce, A., Pascual, J., Toranzo, A. E. & Romalde, J. L. *Vibrio gallaecicus* sp. nov. isolated from cultured clams in north-western Spain. *Sys Appl Microbiol* **32**, 111-117, doi:https://doi.org/10.1016/j.syapm.2008.12.002 (2009).

112 Gomez-Gil, B. *et al. Vibrio sinaloensis* sp. nov., isolated from the spotted rose snapper, *Lutjanus guttatus* Steindachner, 1869. *Int J Sys Evol Microbiol* **58**, 1621-1624, doi:https://doi.org/10.1099/ijs.0.65719-0 (2008).

113 Gómez-León, J., Villamil, L., Lemos, M. L., Novoa, B. & Figueras, A. Isolation of *Vibrio alginolyticus* and *Vibrio splendidus* from aquacultured carpet shell clam (*Ruditapes decussatus*) larvae associated with mass mortalities. *Appl Environ Microbiol* **71**, 98-104, doi:10.1128/aem.71.1.98-104.2005 (2005).

114 BORREGO, J. J. *et al. Vibrio tapetis* sp. nov., the causative agent of the brown ring disease affecting cultured clams. *Int J Sys Evol Microbiol* **46**, 480-484, doi:https://doi.org/10.1099/00207713-46-2-480 (1996).

115 Thompson, F. L., Thompson, C. C. & Swings, J. *Vibrio tasmaniensis* sp. nov., isolated from Atlantic Salmon (Salmo salar L.). *Sys Appl Microbiol* **26**, 65-69, doi:https://doi.org/10.1078/072320203322337326 (2003).

116 Kojima, H., Watanabe, M. & Fukui, M. *Sulfurivermis fontis* gen. nov., sp. nov., a sulfur-oxidizing autotroph, and proposal of *Thioprofundaceae* fam. nov. *Int J Sys Evol Microbiol* **67**, 3458-3461, doi:https://doi.org/10.1099/ijsem.0.002137 (2017).

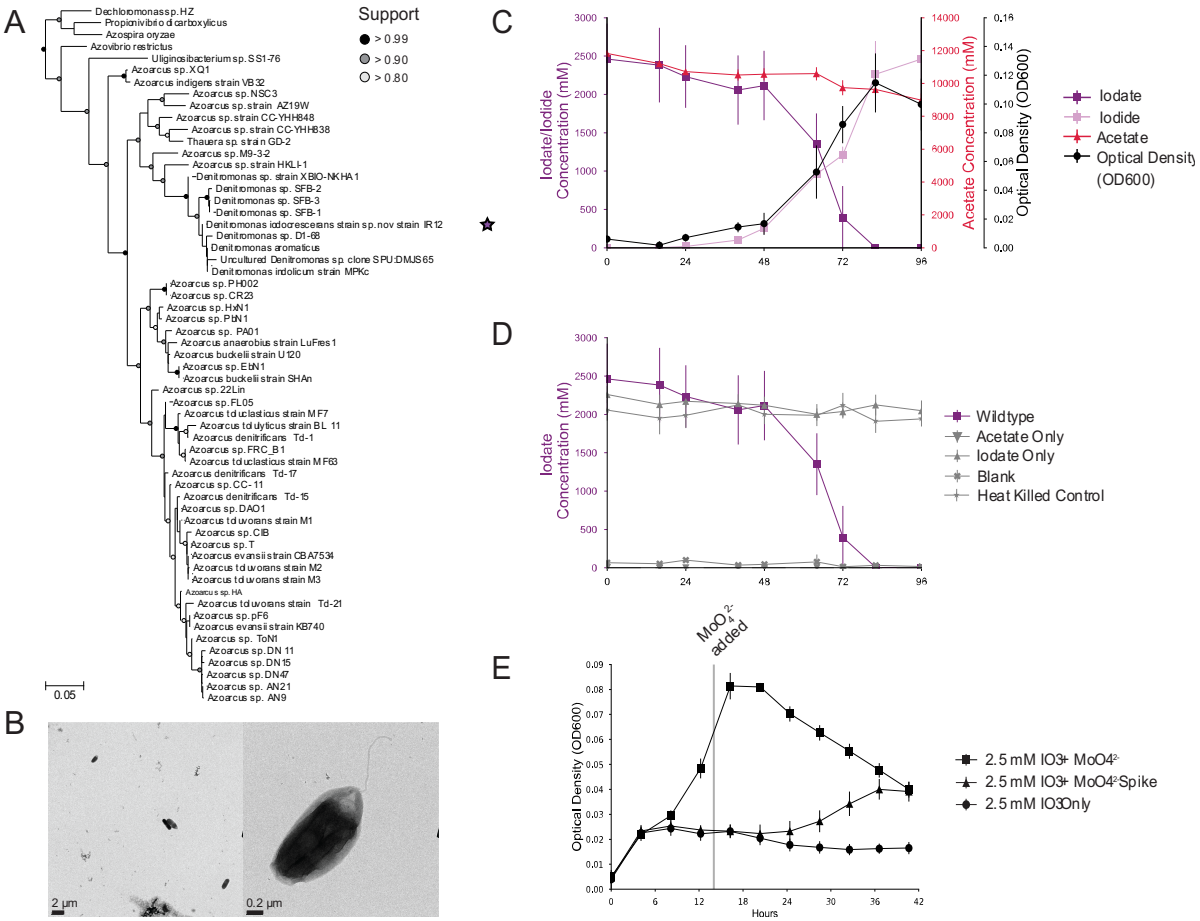

Figure 1: Phylogeny and Physiology of Denitromonas iodocrescerans

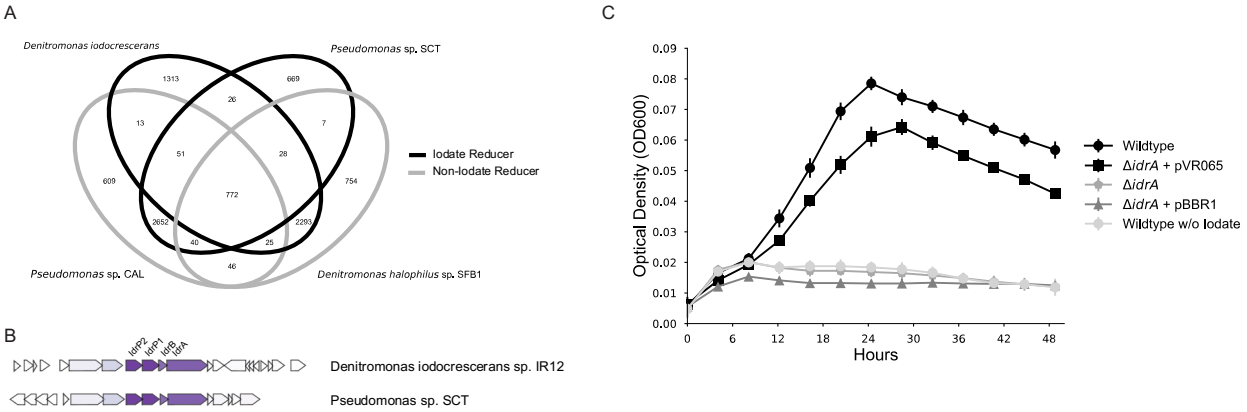

Figure 2: Identification unique gene cluster in iodate reducing genomes enables the identification and characterization of the iodate reductase (IdrA)

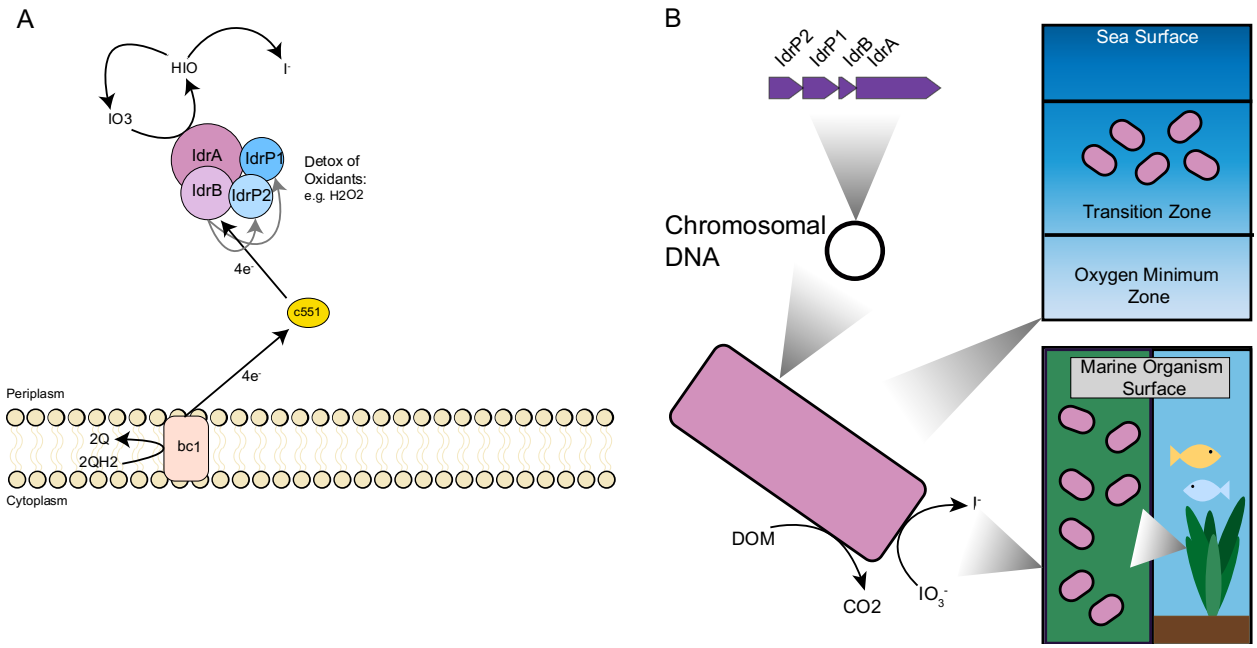

Figure 3 Mechanistic and Ecological Models of Iodate Reduction

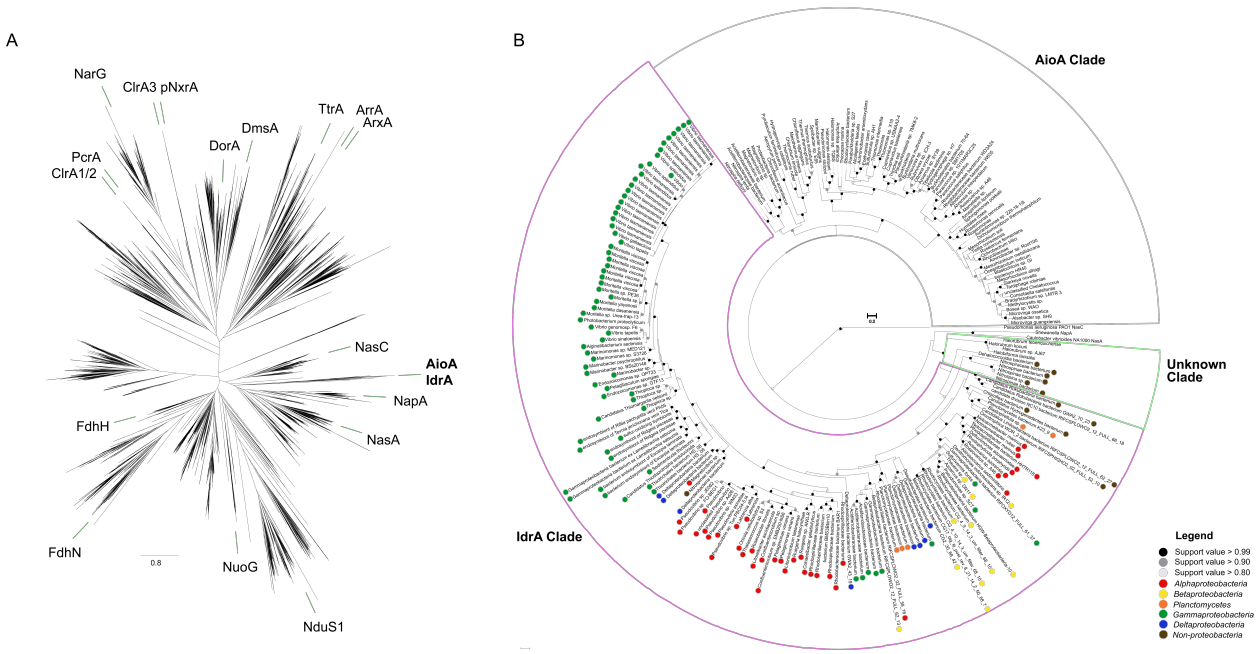

Figure 4 Phylogeny and Taxonomic Distribution of IdrA

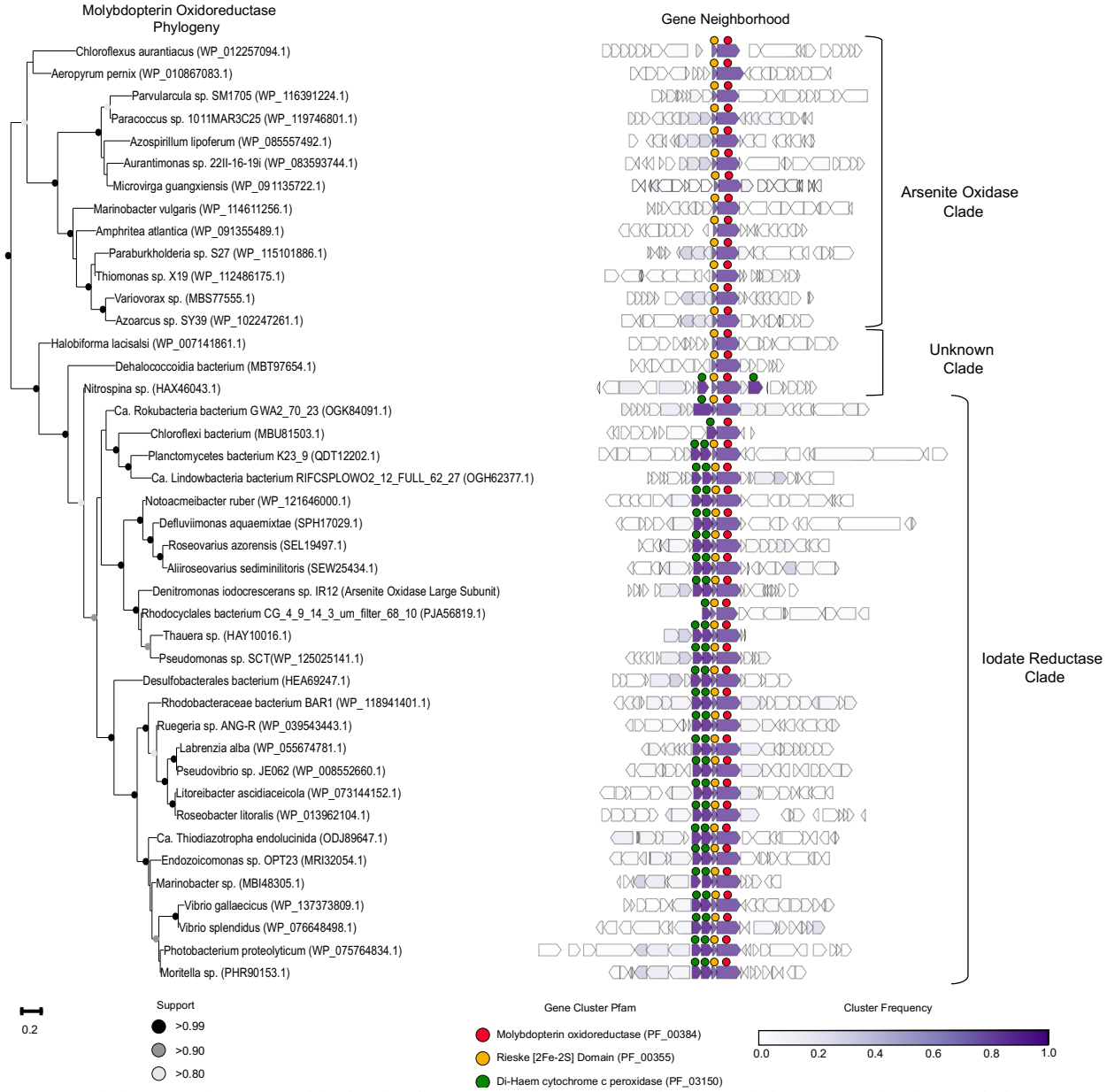

Figure 5 Phylogeny and Gene Neighborhoods of arsenite oxidase, iodate reductase, and the associated unknown clade

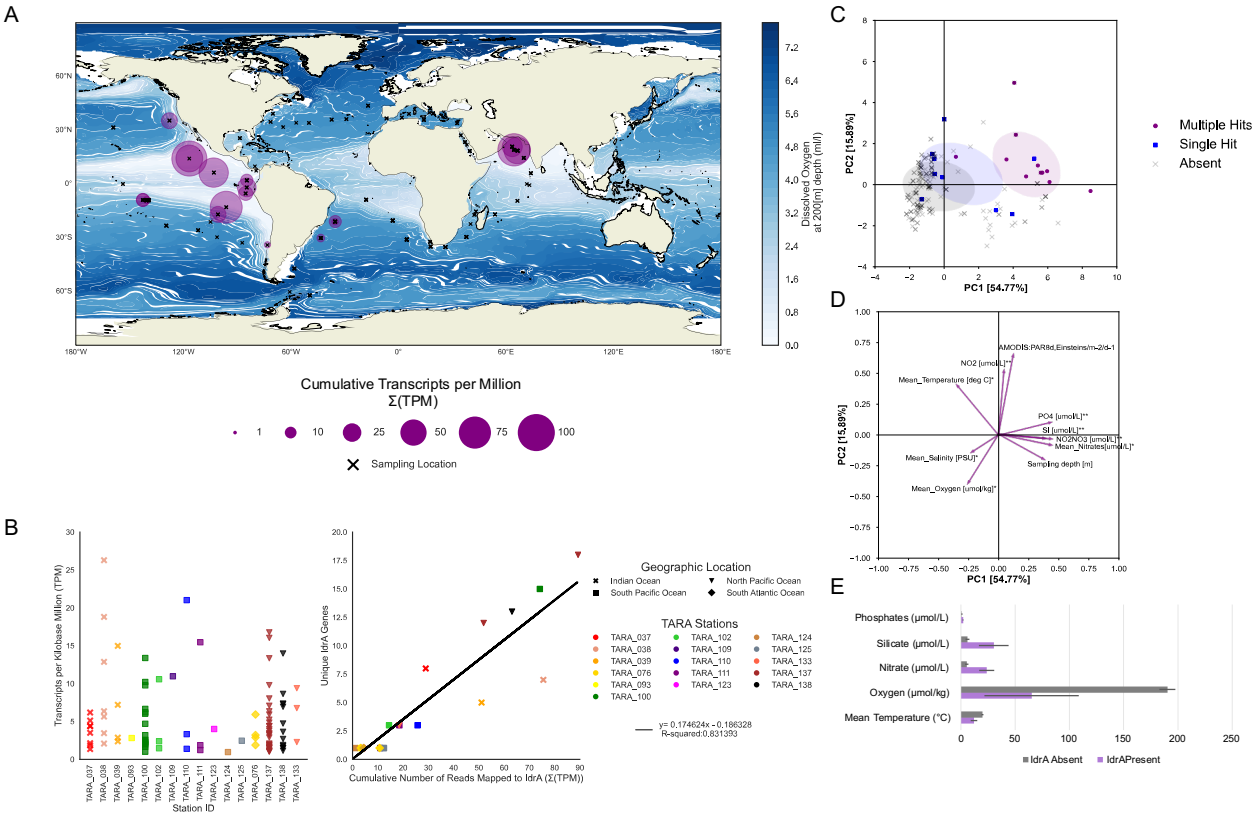

Figure 6 Analysis of Tara Oceans dataset identifies possible ecological niche above oxygen minimum zones